

Decays of Baryon Resonances into ΛK^+ , $\Sigma^0 K^+$ and $\Sigma^+ K^0$

A.V. Sarantsev^{1,2}, V.A. Nikonov^{1,2}, A.V. Anisovich^{1,2}, E. Klempt¹, and U. Thoma^{1,3}

¹ Helmholtz–Institut für Strahlen– und Kernphysik, Universität Bonn, Germany

² Petersburg Nuclear Physics Institute, Gatchina, Russia

³ Physikalisches Institut, Universität Gießen, Germany

June 18, 2018

Abstract. Cross sections, beam asymmetries, and recoil polarisations for the reactions $\gamma p \rightarrow K^+ \Lambda$; $\gamma p \rightarrow K^+ \Sigma^0$, and $\gamma p \rightarrow K^0 \Sigma^+$ have been measured by the SAPHIR, CLAS, and LEPS collaborations with high statistics and good angular coverage for centre-of-mass energies between 1.6 and 2.3 GeV. The combined analysis of these data with data from π and η photoproduction reveals evidence for new baryon resonances in this energy region. A new P_{11} state with mass 1840 MeV and width 140 MeV was observed contributing to most of the fitted reactions. The data demand the presence of two D_{13} states at 1870 and 2170 MeV.

PACS: 11.80.Et, 11.80.Gw, 13.30.-a, 13.30.Ce, 13.30.Eg, 13.60.Le 14.20.Gk

1 Introduction

A quantitative approach to strong interactions at low energies can not be constructed without detailed information about the properties of strongly interacting particles. In recent years, substantial progress had been achieved in understanding the spectrum and the properties of low mass mesons; the observations of new mesons consisting of heavy quarks is one of the hottest topics in hadron physics. However, an understanding of the interaction between quarks can hardly be reached on the basis of knowing only quark–antiquark systems. Only baryons can provide information if pairs of quarks like to cluster into diquarks or if their excitation spectrum unravels the full richness of three–particle dynamics. But at present, only the low–mass baryon resonances are reasonably well established experimentally [1], even though the nature of some of these states is still under discussion. In particular there is no consensus if the Roper $N(1440)P_{11}$, the $N(1535)S_{11}$, and the $\Lambda(1405)S_{01}$ resonances should be interpreted as excited three–quark states or if they are created by conventional or chiral meson–baryon interactions [2, 3, 4, 5, 6, 7, 8, 9]. Above 1.8 GeV, data become sparse, and even the density of states is unclear [10].

Photoproduction of nucleon resonances in their decay to strange particles offers attractive possibilities. In the reaction $\gamma p \rightarrow \Lambda K^+$, only N^* and no Δ^* resonances can contribute. The reactions $\gamma p \rightarrow \Sigma^0 K^+$ and $\gamma p \rightarrow \Sigma^+ K^0$ contribute to both the N^* and Δ^* series, but with different couplings (due to different Clebsch–Gordan coefficients). Since baryon resonances have large widths and are often overlapping, a reduction in the number of partial waves

or/and rigid constraints between different data sets facilitates greatly the task to identify the leading contributions.

Some of the ‘missing’ resonances are predicted to couple strongly to ΛK and ΣK [11] hence they may contribute significantly to these particular channels. Furthermore, Λ ’s reveal their polarisation in their decay, so that polarisation variables are accessible without use of a polarised photon beam or a polarised target. The same is true for the ΣK reaction through the $\Sigma^0 \rightarrow \Lambda \gamma$ decay. And, last not least, high statistics photoproduction data are now available from SAPHIR [12], CLAS [13], and LEPS [14]. In this letter we present results of a partial wave analysis of these data, point out differences between the data and common features. The SAPHIR data on reaction $\gamma p \rightarrow K^0 \Sigma^+$ [15] were finalized only after completion of most of the fits described here. They are not included in the systematic evaluation of errors but only in the final fit. The changes in pole position and helicity couplings induced by the new SAPHIR data are marginal only.

Data on meson production off nucleons have been interpreted using different approaches. Feuster and Mosel developed a unitary effective Lagrangian model and described both meson– and photon–induced reactions on the nucleon. Data involving known baryon resonances of spin $J \leq 3/2$ and later $J \leq 5/2$ were fitted and γN , πN , $\pi \pi N$, ηN and $K \Lambda$ partial widths were extracted [16, 17, 18, 19, 20]. The data have also been interpreted by Regge–model calculations [21] using only K and K^* exchanges and no s –channel resonances. Only the gross features of the data were reproduced. Two models based on similar effective Lagrangian approaches [22, 23, 24] gave the correct order of magnitude of the total cross section but failed to reproduce differential cross sections. A structure near 1.9 GeV was interpreted [23] as evidence for a ‘missing’ resonance

at this mass. Quantum numbers D_{13} were tentatively assigned to the structure which seemed consistent with the angular distribution and quark model prediction [11]. Including data on $K^0 \Sigma^+$ required adding the $N(1720)P_{13}$ resonance [25]. In a more recent analysis [26], the structure finds a more complex interpretation, and the D_{13} partial wave is found to be resonant at 1740 MeV and at a higher ill-defined mass. Janssen et al. [27] do not see the need for introducing a $N(1895)D_{13}$ resonance. Other groups [28, 29] find evidence for a third S_{11} resonance which has been suggested to explain an anomaly in the η photoproduction cross section [30]. Usov and Scholten [31] use a coupled channel frame derived from an effective Lagrangian to fit CLAS and SAPHIR data on ΛK^+ and ΣK . Eight N^* and 3 Δ^* resonances are introduced, among them two P_{11} resonances at 1520 and 1850 MeV and a $\Delta(1855)P_{33}$. The CLAS collaboration concluded that interference between several resonant states must be important in this mass range, rather than a single well-separated resonance.

The partial wave analysis presented here is based on the operator expansion method described in detail in [32]. The method is very convenient to describe s -channel resonances, to calculate contributions from triangle and box diagrams and to project t - and u -channel exchange amplitudes into s -channel partial waves. The data on ΛK^+ and ΣK were fitted jointly with data on π^0 and η photoproduction (see Table 1). Included were the differential cross section for π^0 and η production from CB-ELSA [33, 34], the Mainz-TAPS data [35] on η photoproduction, cross sections for π^0 and η photoproduction from GRAAL and beam asymmetry measurements [36, 37, 38], and data on

Table 1. Data used in the partial wave analysis, χ^2 contributions and fitting weights.

Observable	N_{data}	χ^2	χ^2/N_{data}	Weight	Ref.
$\sigma(\gamma p \rightarrow \Lambda K^+)$	720	804	1.12	4	[12]
$\sigma(\gamma p \rightarrow \Lambda K^+)$	770	1282	1.67	2	[13]
$P(\gamma p \rightarrow \Lambda K^+)$	202	374	1.85	1	[13]
$\Sigma(\gamma p \rightarrow \Lambda K^+)$	45	62	1.42	15	[14]
$\sigma(\gamma p \rightarrow \Sigma^0 K^+)$	660	834	1.27	1	[12]
$\sigma(\gamma p \rightarrow \Sigma^0 K^+)$	782	2446	3.13	1	[13]
$P(\gamma p \rightarrow \Sigma^0 K^+)$	95	166	1.76	1	[13]
$\Sigma(\gamma p \rightarrow \Sigma^0 K^+)$	45	20	0.46	35	[14]
$\sigma(\gamma p \rightarrow \Sigma^+ K^0)$	48	104	2.20	2	[13]
$\sigma(\gamma p \rightarrow \Sigma^+ K^0)$	120	109	0.91	5	[15]
$\sigma(\gamma p \rightarrow p\pi^0)$	1106	1654	1.50	8	[33]
$\sigma(\gamma p \rightarrow p\pi^0)$	861	2354	2.74	3.5	[36]
$\Sigma(\gamma p \rightarrow p\pi^0)$	469	1606	3.43	2	[36]
$\Sigma(\gamma p \rightarrow p\pi^0)$	593	1702	2.87	2	[37]
$\sigma(\gamma p \rightarrow n\pi^+)$	1583	4524	2.86	1	[39]
$\sigma(\gamma p \rightarrow p\eta)$	667	608	0.91	35	[34]
$\sigma(\gamma p \rightarrow p\eta)$	100	158	1.60	7	[35]
$\Sigma(\gamma p \rightarrow p\eta)$	51	114	2.27	10	[38]
$\Sigma(\gamma p \rightarrow p\eta)$	100	174	1.75	10	[36]

$\gamma p \rightarrow n\pi^+$ [39]. The different data sets enter the fits with weights which are listed in the fifth column of Table 1. The fits minimise a pseudo-chisquare function

$$\chi_{\text{tot}}^2 = \frac{\sum w_i \chi_i^2}{\sum w_i N_i} \sum N_i. \quad (1)$$

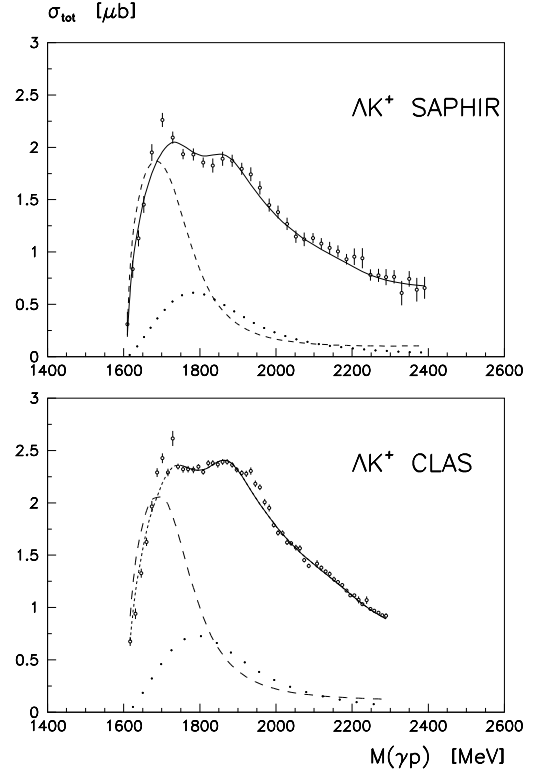


Fig. 1. The total cross sections as a function of $W = M_{\gamma p}$ for for ΛK^+ photoproduction measured by SAPHIR [12] and CLAS [13]. The solid curves are results of our fit. Dashed lines show the contribution from S_{11} K -matrix amplitude, dotted lines show the contribution from $P_{13}(1720)$. The prediction of the total cross section in the region where data were not used for the fit is shown as short-dashed line. The discrepancy at $M_{\gamma p} \sim 1.7$ GeV is discussed in section 2.1.

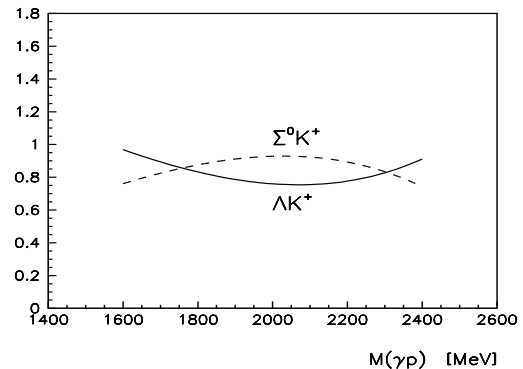


Fig. 2. Energy dependent normalisation factor, the solid line is for the ΛK^+ data and the dashed line is for the ΣK data. The fit result was multiplied by the factor before it was compared with the SAPHIR data.

where the N_i are given as N_{data} (per channel) in the second and the weights in the last column of Table 1.

The partial wave solutions based on π^0 and η photoproduction data only were presented earlier in the two letter publications [33,34]. Aspects of the new fits related to the π^0 and η photoproduction are presented in the preceding paper [40]. In this paper, those results are discussed which pertain to final states with open strangeness.

2 Photoproduction of open strangeness

2.1 ΛK^+ photoproduction

The CLAS data cover the mass (\sqrt{s}) range from the $K\Lambda$ threshold to 2.4 GeV. The differential angular distributions are given in 56 bins about 13 MeV wide at low energies and 10 MeV wide at high energies. The SAPHIR collaboration showed 36 angular distributions from threshold to 2.4 GeV in about 20 MeV wide mass bins. The CLAS and SAPHIR data are complemented by the coincident observation of the Λ recoil polarisation. The LEPS collaboration at SPring-8 published beam asymmetry measurements in 9 mass bins covering the same mass range.

The experimental total cross section was determined by summation of the experimental differential cross sections and, in regions where no data exist, predicted values determined by the fit. For some very forward SAPHIR data points, fit values were taken as well.

The SAPHIR and CLAS $\gamma p \rightarrow \Lambda K^+$ total cross sections show a very narrow enhancement in the 1700 MeV region. It can easily be fitted by giving the $N(1650)S_{11}$ resonance a narrow (~ 30 MeV) width or by introducing a new S_{11} or P_{11} resonance (where the former resonance

gives a slightly better description). If such a state exists, it couples strongly only to the ΛK^+ channel and must have a very exotic nature. While the narrow peaks seem to be consistent in the SAPHIR and CLAS total cross sections, their origin is very different. In the SAPHIR data, the peak is connected with a larger differential cross section (compared to the fit) over a broad angular range; in the CLAS data, the peak originates from just two points in the very forward region. If these points are excluded, the CLAS total cross section is even smaller than given by the fit. Of course, a new narrow state should not be claimed on this basis; new data are needed to resolve this discrepancy and the narrow structure at 1700 MeV is disregarded here.

The Figs. 3 and 4 show the differential cross sections obtained by SAPHIR and CLAS and the results of the best fit described below. The agreement is rather good in both cases: most discrepancies between the two experiments can obviously be ascribed to an overall energy-dependent normalisation error.

The beam polarisation asymmetries are compared to the fit in Fig. 5. For these data, the calculations were made for narrow bins (with ten times smaller widths) and then

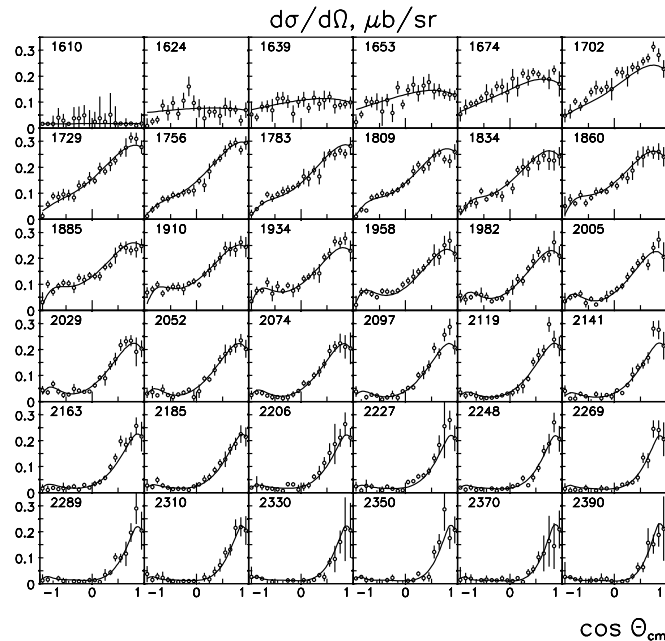


Fig. 3. The angular distributions as a function of W for $\gamma p \rightarrow \Lambda K^+$, SAPHIR data.

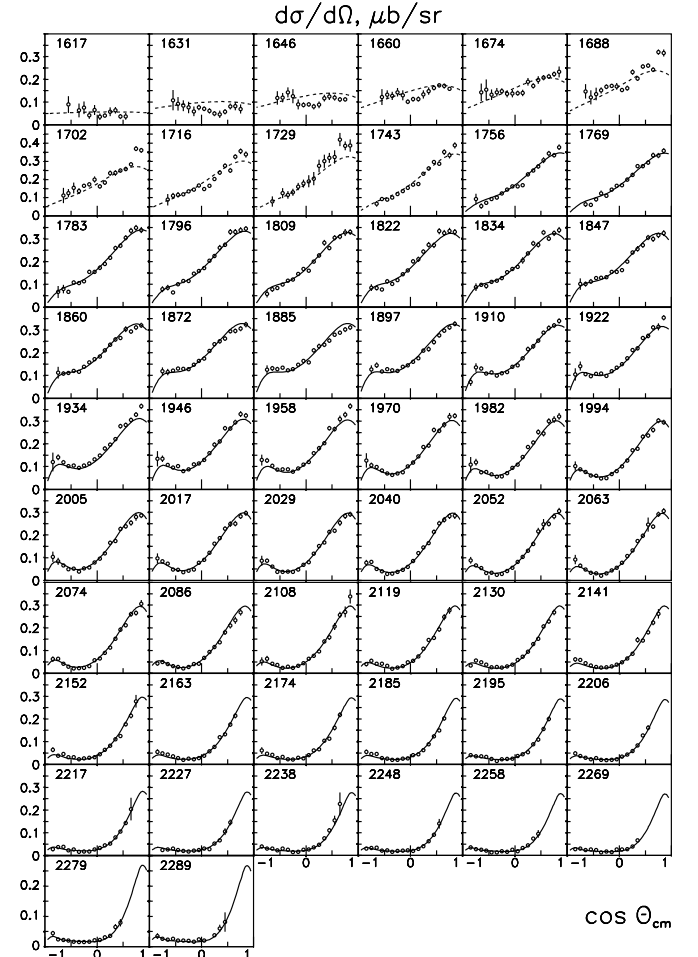


Fig. 4. The angular distributions as a function of W for $\gamma p \rightarrow \Lambda K^+$, CLAS data. The prediction for the region where data were not used in the fit is shown as dashed lines.

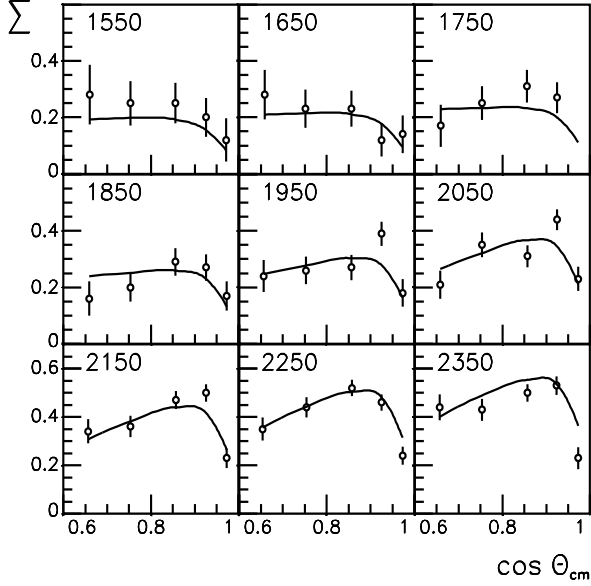


Fig. 5. The beam polarisation asymmetries as a function of W for $\gamma p \rightarrow K^+ \Lambda$ [14]. The curves are the result of our fit.

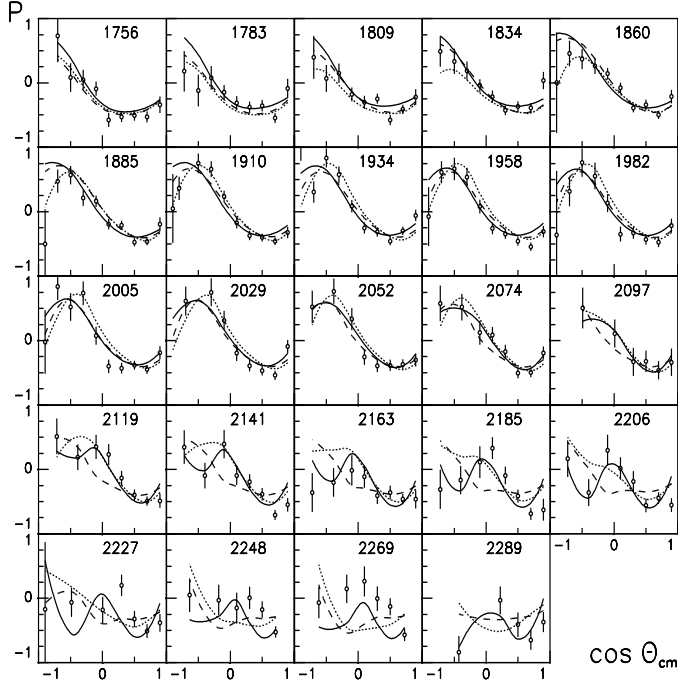


Fig. 6. Recoil polarisation of Λ hyperons as a function of W for the center-of-mass kaon angle $\cos(\theta_K^{CM})$. The vertical bars on CLAS data (solid points) combine statistical and systematic errors. The solid line presents our fit. The dashed curves represent results when the $N(2170)D_{13}$ is omitted, for the dotted lines the $N(1840)P_{11}$ was omitted in the fit.

averaged to fit the correspondent experimental data. The recoil polarisation, obtained from the weak-decay asymmetry of hyperons, provides further constraints to the solution. Data and fit, divided into 24 mass bins, are shown in Fig. 6.

2.2 ΣK photoproduction

The $\gamma p \rightarrow \Sigma K$ data obtained by CLAS and SAPHIR cover the same energy range as the $\gamma p \rightarrow \Lambda K^+$ data. The data are also complemented by the coincident observation of the Σ recoil polarisation. The beam asymmetry was measured by LEPS and given in 9 energy intervals covering the same mass range as the ΛK^+ measurements. The CLAS data for $\Sigma^+ K^0$ photoproduction [41] are binned into 6 energy intervals of about 100 MeV width. This data is also used in the fits. The calculations were made for 10 MeV mass spacings and then averaged to fit the experimental bins.

As in the case of the ΛK^+ reactions, the total cross section measurements from SAPHIR and CLAS are not fully compatible. In Fig. 7 the different height of the total cross sections as obtained by the two experiments can be seen. Both data agree only after renormalisation with an energy dependent function as given in Fig. 2.

The SAPHIR and CLAS differential cross sections $\Sigma^0 K^+$ and the result of the best fit are shown in Figs. 8 and 9. The agreement is rather good in both cases: as for ΛK^+ production, the discrepancy can be ascribed to an overall

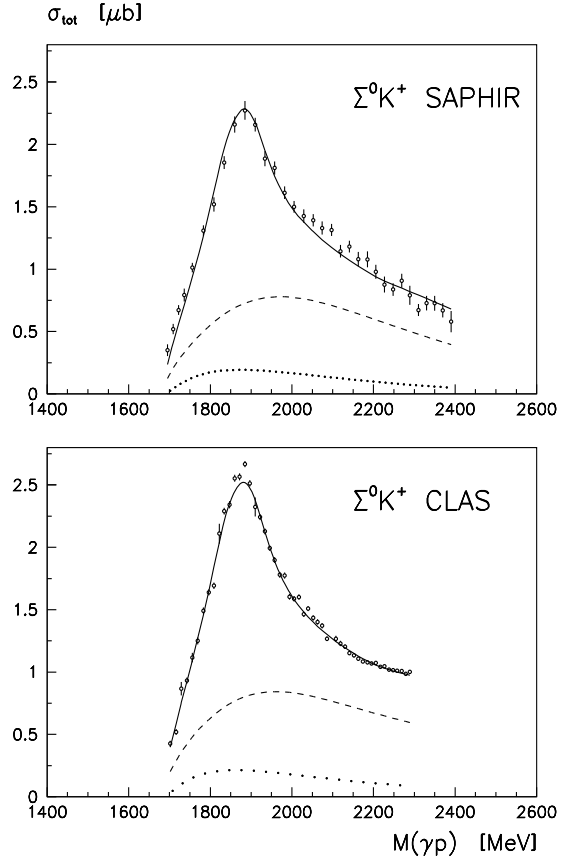


Fig. 7. Total cross sections for $\Sigma^0 K^+$ photoproduction measured at SAPHIR [12] and CLAS [13]. The solid curves are results of our fit. The total cross section was determined in the same way as for ΛK^+ channel. Dashed lines show the contribution from K^* -exchange, dotted lines the contribution from $D_{33}(1700)$.

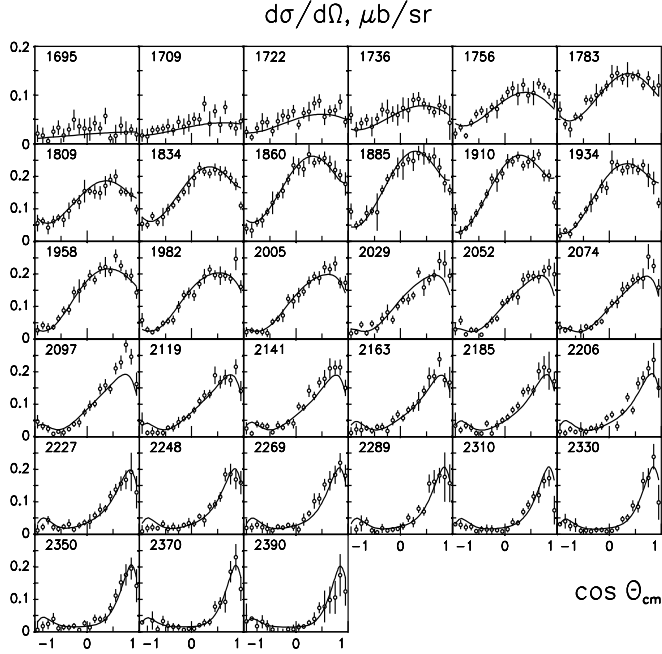


Fig. 8. Angular distributions for $\gamma p \rightarrow K^+ \Sigma^0$, SAPHIR data [12].

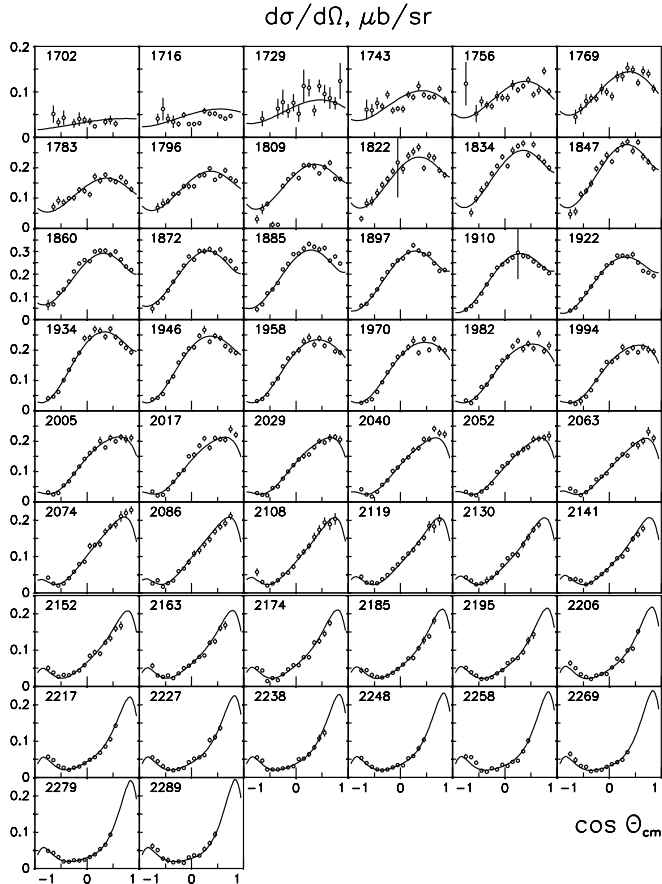


Fig. 9. Angular distributions for $\gamma p \rightarrow K^+ \Sigma^0$, CLAS data [13].

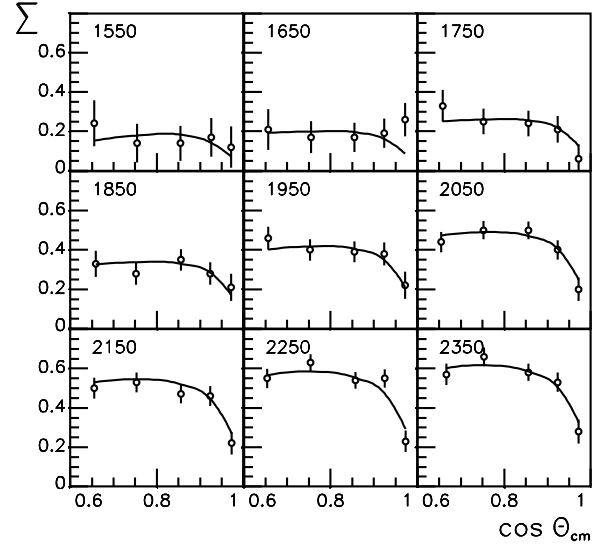


Fig. 10. Beam polarisation asymmetries for $\gamma p \rightarrow K^+ \Sigma$, LEPS data.

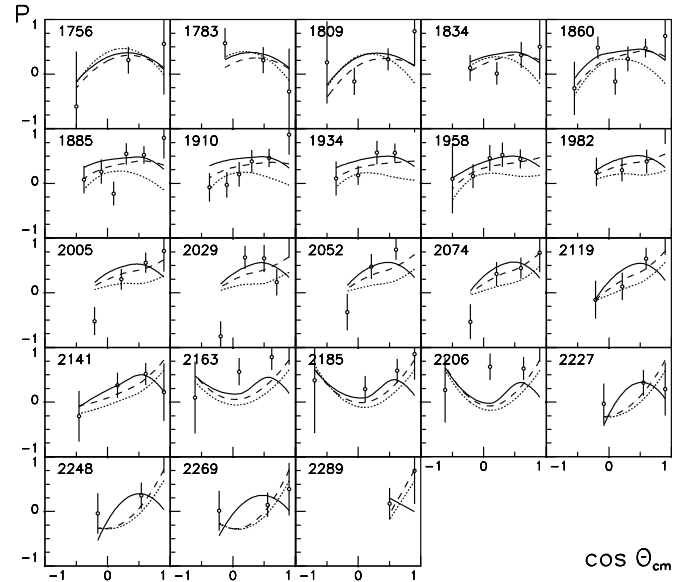


Fig. 11. Recoil polarisations for $K^+ \Sigma^0$, CLAS data. The solid curves are results of the fit. The dashed curves correspond to the solution without $N(2170)D_{13}$ and the dotted curves to the solution without $(1840)P_{11}$.

energy-dependent normalisation error. The beam polarisation asymmetries from LEPS are given in Fig. 10 and the Σ recoil polarisation data divided into 23 energy bins are shown in Fig. 11.

The total and differential cross sections $\Sigma^+ K^0$ versus our fit are given in Figs. 12. In this case, no normalisation factor was applied.

2.3 The normalisation function

Finally, a comment seems appropriate concerning the inconsistency between total cross section obtained by the

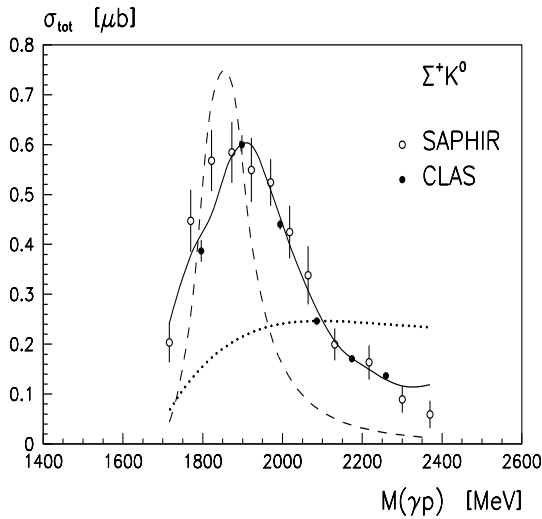


Fig. 12. The total cross sections for $K^0 \Sigma^+$ photoproduction. The solid curve represents our fit. The SAPHIR cross section is shown as open circles. For the CLAS data the experimental total cross section (full circles) was determined by summation of the experimental differential cross sections and, in regions where no data exist, predicted values determined by the fit. Dashed line shows the contribution from $P_{11}(1840)$, dotted line shows the contribution from Σ -exchange.

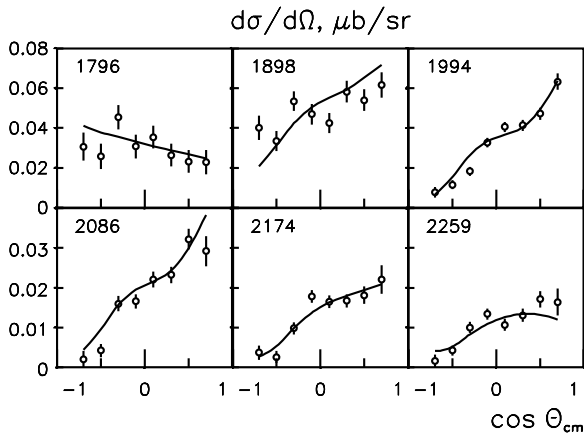


Fig. 13. Angular distributions for $K^0 \Sigma^+$ CLAS data

SAPHIR and CLAS collaborations. If the problem is connected with an error in the photon flux normalisation, the normalisation factor should not depend on energy. A fit with an energy independent factor increased χ^2 for $\gamma p \rightarrow \Lambda K^+$ by 16 for the SAPHIR differential cross sections, and by 40 for the CLAS differential cross sections. The recoil polarisation data were described by a curve with an increase of χ^2 by 20. Such small differences are not seen in the pictures, and we conclude that the energy dependence does not play any critical role. The total χ^2 for ΣK final states only changed by 20. A constant normalisation factor was determined to be 0.80 for $\gamma p \rightarrow \Lambda K^+$ and 0.89 for $\gamma p \rightarrow \Sigma K$. If all reactions were fitted with the same factor, it optimised at 0.82 ± 0.03 . This factor is very close to that obtained for the ΛK^+ channel, and the χ^2 changed only by another 20. However, the calculated ΣK total cross section was then systematically lower than the

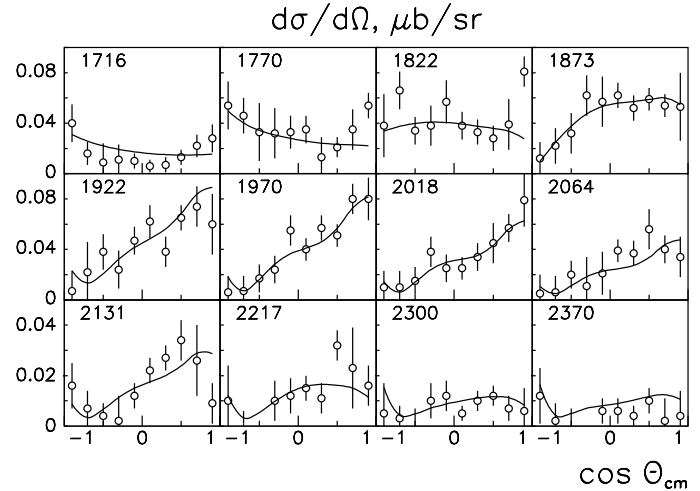


Fig. 14. Angular distributions for $K^0 \Sigma^+$ SAPHIR data

SAPHIR data points. In any case, including or excluding the energy dependence of the normalisation factor does not change any of the conclusions concerning masses or widths of baryon resonances.

3 Fit results

The fitting weights of the various data sets and their χ^2 contributions are given in Table 1. The weights of the ΛK^+ and ΣK data were selected to obtain a good description of this data without noticeable deterioration of the fit to π and η . The solution was carefully checked for stability. The weights of some channels were changed significantly, the resulting changes in the fit parameters were included in the final systematic errors. For example, increasing the weights from 3 to 35 for the data on beam asymmetry improved the description of this data, increased slightly the χ^2 for other data, but lead to very small (maximum 5 MeV) shifts in resonance positions and/or widths.

3.1 First fits

In first fits, all resonances seen in the analysis of π^0 and η photoproduction [33,34] were introduced in the fit. Unphysical solutions were obtained in some of the fits, and couplings of resonances had to be restricted. The ΣK data have a rather pronounced peak in the 1800 MeV mass region; some solutions described the peak by a single resonance having a huge coupling to this channel. This amplitude created large interferences with other contributions. To avoid this class of solutions, we demanded that the ΛK^+ and ΣK couplings should not exceed the couplings to the πp or ηp channels by more than a factor 2. In this way, solutions were found producing an acceptable overall description of the data with χ^2 values very close to the best fit not having such restrictions. In the new fits, all resonances had couplings well within the boundaries. When a coupling constant fell onto a boundary value, the fit was not sensitive to this coupling.

Table 2. Masses, widths and coupling constants squared for N^* and Δ^* resonances. The values are given for the best fit and errors cover systematical errors. Normalisation condition for Breit–Wigner resonances is $\sum g_i^2 = 1$. The errors are estimated from a variety of different solutions.

Resonance	M (MeV)	Γ (MeV)	$g_{\text{N}\pi}^2$	$g_{\text{N}\eta}^2$	$g_{\Lambda\text{K}}^2$	$g_{\Sigma\text{K}}^2$
N(1440) P_{11}	1450 ± 50	250 ± 150	1	-	-	-
PDG	1440^{+30}_{-10}	350 ± 100				
N(1520) D_{13}	1526 ± 4	112 ± 10	0.62 ± 0.06	0.04 ± 0.03	0.03 ± 0.02	0.31 ± 0.09 **
PDG	1520^{+10}_{-5}	120^{+15}_{-10}				
N(1535) S_{11}^*	1530 ± 30	210 ± 30	0.39 ± 0.10	0.95 ± 0.20	0.30 ± 0.10	0.30 ± 0.10 **
PDG	1505 ± 10	170 ± 80				
N(1650) S_{11}^*	1705 ± 30	220 ± 30	1.10 ± 0.20	0.40 ± 0.10	0.10 ± 0.10	0.50 ± 0.15
PDG	1660 ± 20	160 ± 10				
N(1675) D_{15}	1670 ± 20	140 ± 40	0.32 ± 0.15	0.04 ± 0.04	0.39 ± 0.20	0.25 ± 0.20
PDG	1675^{+10}_{-5}	150^{+30}_{-10}				
N(1680) F_{15}	1667 ± 6	102 ± 15	$0.95^{+0.05}_{-0.10}$	$0.00^{+0.05}_{-0.00}$	$0.05^{+0.10}_{-0.05}$	$0.00^{+0.05}_{-0.00}$
PDG	1680^{+10}_{-5}	130 ± 10				
N(1700) D_{13}	1725 ± 15	100 ± 15	0.29 ± 0.15	0.51 ± 0.15	0.13 ± 0.10	$0.07^{+0.12}_{-0.07}$
PDG	1700 ± 50	100 ± 50				
N(1720) P_{13}	1750 ± 40	380 ± 40	0.39 ± 0.10	0.43 ± 0.12	0.16 ± 0.05	0.02 ± 0.02
PDG	1720^{+30}_{-70}	250 ± 50				
N(1840) P_{11}	1840^{+15}_{-40}	140^{+30}_{-15}	0.31 ± 0.10	0.09 ± 0.05	0.06 ± 0.03	0.54 ± 0.10
PDG	1720 ± 30	100^{+150}_{-50}				
N(1870) D_{13}	1875 ± 25	80 ± 20	0.04 ± 0.04	0.21 ± 0.10	0.03 ± 0.03	0.72 ± 0.30
N(2000) F_{15}	1850 ± 25	225 ± 40	0.85 ± 0.20	$0.07^{+0.11}_{-0.07}$	$0.03^{+0.07}_{-0.03}$	$0.05^{+0.10}_{-0.05}$
PDG	~ 2000					
N(2070) D_{15}	2060 ± 30	340 ± 50	0.71 ± 0.10	0.26 ± 0.05	0.01 ± 0.01	0.02 ± 0.02
N(2170) D_{13}	2166^{+25}_{-50}	300 ± 65	0.67 ± 0.30	0.15 ± 0.05	0.16 ± 0.15	$0.14^{+0.15}_{-0.14}$
PDG	~ 2080					
N(2200) P_{13}	2200 ± 30	190 ± 50	$0.08^{+0.12}_{-0.08}$	$0.89^{+0.08}_{-0.15}$	$0.02^{+0.08}_{-0.02}$	$0.01^{+0.08}_{-0.01}$
$\Delta(1232)\text{P}_{33}$	1235 ± 4	140 ± 12	1			-
PDG	1232 ± 2	120 ± 5				
$\Delta(1620)\text{S}_{31}$	1635 ± 6	106 ± 12	1.00 ± 0.10			$0.0^{+0.10}_{-0.00}$
PDG	1620^{+55}_{-5}	150 ± 30				
$\Delta(1700)\text{D}_{33}$	1715 ± 20	240 ± 35	0.78 ± 0.15			0.22 ± 0.15
PDG	1700^{+70}_{-30}	300 ± 100				
$\Delta(1905)\text{F}_{35}$	1870 ± 50	370 ± 110	0.90 ± 0.10			0.10 ± 0.10
PDG	1905^{+15}_{-35}	350^{+90}_{-70}				
$\Delta(1920)\text{P}_{33}$	1996 ± 30	380 ± 40	$0.94^{+0.06}_{-0.10}$			$0.06^{+0.10}_{-0.06}$
PDG	1920^{+50}_{-20}	250^{+100}_{-50}				
$\Delta(1940)\text{D}_{33}$	1930 ± 40	200 ± 100	0.32 ± 0.30			0.68 ± 0.30
$\Delta(1950)\text{F}_{37}$	1893 ± 15	240 ± 30	0.90 ± 0.10			0.10 ± 0.10
PDG	1950 ± 10	300^{+50}_{-10}				

* K matrix fit, the position of the amplitude poles in the complex planes closest to the physical region.

** See text for discussion of the large values of $g_{\Sigma\text{K}}^2$.

In some particular mass regions, the fit deviated visibly from the data. These regions are now discussed in some detail. The discussion will lead to the final fit and to the results gathered in Table 2.

To estimate systematic errors, fits were performed excluding the SAPHIR or CLAS cross sections. Masses and widths of the resonances of the main solution are defined more precisely by the CLAS data; masses and widths changed by less than 4 MeV in the fit with the SAPHIR data excluded. If the CLAS cross sections were excluded, a few more significant changes of the resonance positions were found. All these uncertainties are included in the errors given in Table 2.

In Table 3 we give ratios of partial widths derived from the couplings given in Table 2. The relation between coupling constants and partial widths is given e.g. in eq. (11) of the preceding paper [40].

3.2 The low-mass region (1500–1750 MeV)

The cross section for the reaction $\gamma p \rightarrow \Lambda K^+$ rises steeply above threshold and reaches a maximum value at about 1720 MeV, just 100 MeV above the ΛK^+ threshold. The peak cross section for $\gamma p \rightarrow \Sigma K$ is reached only at about 1900 MeV. This behaviour suggests that near-threshold resonances should have strong couplings to ΛK^+ . The fit gives, however, stronger subthreshold couplings to the ΣK channel. These strong subthreshold ΣK couplings parameterise a background which interferes near threshold with t - and u -channel exchanges.

The low-mass part is strongly influenced by the S_{11} partial wave, in particular by $N(1650)S_{11}$. As mentioned, the S_{11} partial wave is described by a two-pole four-channel K -matrix. The lower K -matrix pole can have its position in a very wide mass interval, in some fits it moved down to 1100 MeV. However, there is no visible

change in the fit as long as the K -matrix pole is situated between 1200 and 1460 MeV. For K -matrix masses above 1400 MeV, the fit started to exceed the SAPHIR total cross section for $\gamma p \rightarrow \Lambda K^+$ at ~ 1850 MeV, but the CLAS data were described more precisely. The K -matrix pole is obviously defined only with an appreciable error, we quote (1440^{+40}_{-180}) MeV. There is a strong dependence of the low mass K -matrix pole couplings on the pole position. For example when the mass of lowest K -matrix pole goes to lower values the ΣK coupling increased very significantly providing the same overall S_{11} contribution to the ΣK cross section.

The T -matrix poles are studied in the \sqrt{s} complex plane. Due to the four-channel nature, the complex plane is split into 8 Riemann sheets, 4 of them are relevant for the discussion. The pole positions of the T -matrix amplitude are given in Table 2 together with squared K -matrix couplings. The analytical continuation of

$$\rho_a(s) = \frac{\sqrt{(s - (m_\mu + m_B)^2))(s - (m_\mu - m_B)^2)}}{s},$$

$$a = \pi N, \eta N, K\Lambda, K\Sigma \quad \mu = \pi, \eta, K \quad B = N, \Lambda, \Sigma \quad (2)$$

to the lower complex s -plane defines the sheet closest to the physical region above threshold, for $Re(s) > (m_\mu + m_B)^2$. For points on this sheet with $Re(s) < (m_\mu + m_B)^2$, the closest physical region is at the threshold. Let us denote this sheet as H . The sheet defined by the analytical continuation of the expression

$$\rho_a(s) = i \frac{\sqrt{((m_\mu + m_B)^2 - s)(s - (m_\mu - m_B)^2)}}{s}$$

is closest to the physical region for $Re(s) < (m_\mu + m_B)^2$; this sheet is denoted as L . The first pole situated on the sheet $HHLL$ with respect to the πN , ηN , $K\Lambda$, and $K\Sigma$ thresholds has a mass $(1534 - i \cdot 107)$ MeV. The correspondent pole situated on the sheet $HHHL$ is very close in mass, $(1518 - i \cdot 121)$ MeV. The second pole has a mass $1710 - i \cdot 105$ MeV and is situated on the sheet $HHHH$. The correspondent pole on the sheet $HHHL$ has a mass of $1703 - i \cdot 115$ MeV. The thresholds situated near poles have only a weak influence on pole positions.

We found that T -matrix poles close to the physical region are very stable when the masses of the K -matrix poles are scanned in a large interval. Only a few minor changes occurred compared to the previous analysis [33, 34] in which a two channel K -matrix was used. The errors given in the Table 2 are defined from a large set of solutions made under different assumptions; changes of the pole positions could even be larger than the errors quoted in the Table, though, when more channels are included.

To estimate unseen contributions from three-body final states, fits were performed with a five-channel K -matrix where the fifth channel provided an unknown inelasticity. It was parametrised as $\pi\pi N$ phase volume. We found negligible contributions from this channel and poor convergence of the fits.

Table 3. Ratios of partial widths

Resonance	$\Gamma_{N\eta}/\Gamma_{N\pi}$	$\Gamma_{\Lambda K}/\Gamma_{N\pi}$	$\Gamma_{\Sigma K}/\Gamma_{N\pi}$
N(1520)D ₁₃	$1.5 \cdot 10^{-3}$	0	0
N(1675)D ₁₅	0.05	0.05	0
N(1680)F ₁₅	$1 \cdot 10^{-3}$	$1 \cdot 10^{-4}$	0
N(1700)D ₁₃	0.80	0.07	$5 \cdot 10^{-3}$
N(1720)P ₁₃	0.80	0.20	0.01
N(1840)P ₁₁	0.25	0.11	0.80
N(1870)D ₁₃	2.0	0.28	1.6
N(2000)F ₁₅	0.04	$5 \cdot 10^{-3}$	$3 \cdot 10^{-3}$
N(2070)D ₁₅	0.30	$8 \cdot 10^{-3}$	0.015
N(2170)D ₁₃	0.04	0.17	0.14
N(2200)P ₁₃	2.0	0.18	0.11
$\Delta(1700)D_{33}$			$2.5 \cdot 10^{-3}$
$\Delta(1920)P_{33}$			0.04
$\Delta(1940)D_{33}$			0.75
$\Delta(1950)F_{37}$			0.01

3.3 The intermediate mass range (1700–2200 MeV)

Small discrepancies were also seen in different distributions in the 1800–1900 MeV mass region. To resolve these discrepancies, resonances with different quantum numbers were added one by one. The most significant improvement came from a P_{11} state with mass (1840^{+15}_{-40}) MeV and width (140^{+35}_{-15}) MeV. With this state included a very satisfactory description of all data sets (except for ΣK polarisation, see below) was obtained up to 2100 MeV. The χ^2 was improved almost for all reactions. The fit of the recoil polarisations without this state (where the effect is clearly visible) is shown as dashed curves in Figs. 6,11. The SAPHIR data on $K^0 \Sigma^+$ production were added at the end of this analysis. They are described with a $\chi^2 = 109$ for 120 data points. The comparison of this solution with resonances having other quantum numbers but a similar mass is made in Table 4.

Fig. 15 a shows a mass scan of the resonance (χ^2 as a function of the assumed P_{11} mass). In the scan, the mass of the P_{11} mass was fixed to preset values while all other fit parameters were allowed to adjust newly. There is a clear χ^2 minimum at 1810–1850 MeV. In Fig. 15 a, the χ^2 changes are shown for the fit of πN and ηN differential cross sections and beam asymmetry data. The P_{11} con-

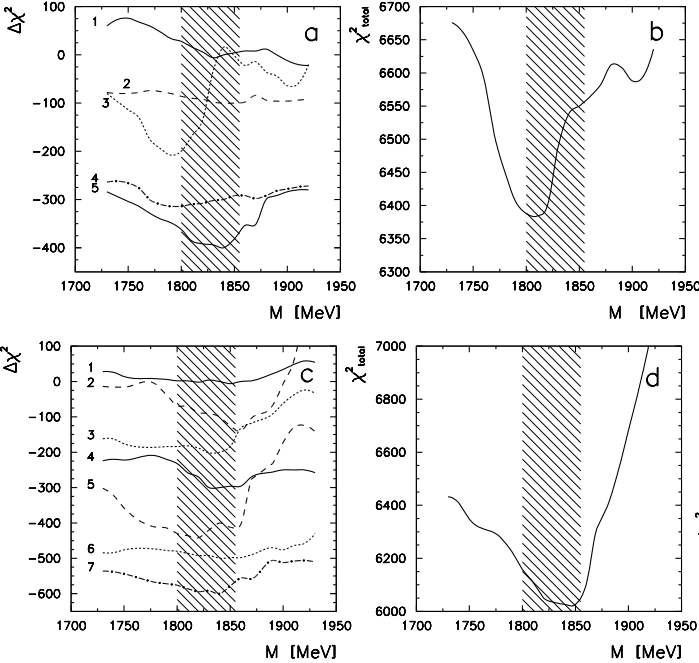


Fig. 15. The result of $P_{11}(1840)$ mass scan: a) 1 – $d\sigma/d\Omega$ for $\gamma p \rightarrow \pi^0 N$ (CB-ELSA) 2 – $d\sigma/d\Omega$ for $\gamma p \rightarrow \eta N$ (CB-ELSA) 3,4 – beam asymmetry for π^0 and η photoproduction (GRAAL), 5 – $d\sigma/d\Omega$ for π^0 photoproduction (GRAAL); b) the sum of χ^2 for the reactions shown in a); c) 1 – the SAPHIR ΛK^+ $d\sigma/d\Omega$, 2 – the CLAS ΛK^+ $d\sigma/d\Omega$, 3 – the ΛK^+ recoil polarization (CLAS), 4 – the SAPHIR ΣK $d\sigma/d\Omega$, 5 – the CLAS ΣK differential cross section, 6 – the ΣK beam asymmetry, 7 – the ΣK recoil polarisation; d) the total χ^2 for all ΛK^+ and ΣK reactions.

tribution leads to a minimum in χ^2 for all individual distributions, although the optimum is slightly lower for the latest GRAAL beam asymmetry data. The changes for the sum of χ^2 for these reactions is shown in Fig. 15 b. The correspondent pictures for the reactions with ΛK^+ and ΣK final states are shown in Figs. 15 c,d. Here the χ^2 distribution as well has a minimum at 1840 MeV almost for all reactions. This fact provides strong evidence that the $N(1840)P_{11}$ is a genuine resonance and not an artefact of some data. The width is determined to be (140^{+35}_{-15}) MeV. This is the minimum value when the width is determined as a function of the fitted mass: if the mass is shifted by 60 MeV from the central position the width increases almost by factor 2.

The $N(1840)P_{11}$ mass is considerably larger than that of the PDG $N(1710)P_{11}$. This is a discrepancy but, possibly, the $N(1710)P_{11}$ could be split into two resonances, an $N(1670)P_{11}$ and an $N(1840)P_{11}$. An $N(1670)P_{11}$ is predicted as member of an antidecuplet [42] and evidence was reported for a narrow resonance at 1670 MeV which might have P_{11} quantum numbers [43]. A mass scan was therefore performed searching for an additional P_{11} state, fixing the mass of $P_{11}(1840)$ at the optimum value. The description of the CLAS differential cross sections in both final channels was slightly improved if this additional resonance had a large mass and a very wide width, but there was no clear minimum in the χ^2 distributions. In the analysis of $\pi N \rightarrow N\pi$ and $N\pi\pi$ the P_{11} mass and width were determined to have values fully compatible with our findings [44].

The recoil polarisation for ΣK production still had systematic deviations between data and fit, and ΛK^+ production showed a discrepancy in the 2.2 GeV mass region. Also the recoil polarisation for $\gamma p \rightarrow \Lambda K^+$ was not well described in the 2.2 GeV mass region. As before resonances with different quantum numbers were introduced one by one. Only adding contributions from the D_{13} wave improved the picture. Two D_{13} states needed to be introduced; the mass of the lower-mass state optimised for (1875 ± 25) MeV and a width of (80 ± 20) MeV. The result of the mass scan for this state is shown in Fig. 16. There is a clear minimum for the GRAAL πN differential cross section and for the ΣK (SAPHIR, CLAS) differen-

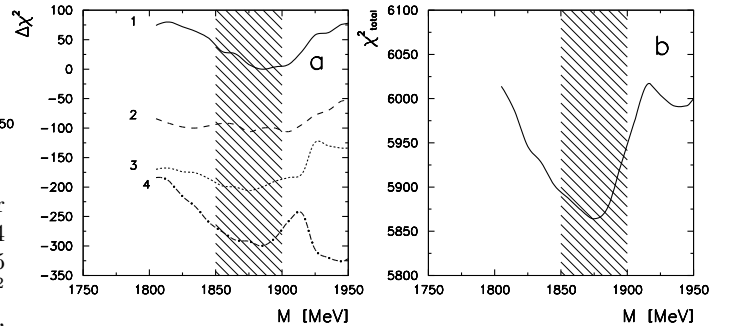


Fig. 16. The result of $D_{13}(1870)$ mass scan: a) 1 – $d\sigma/d\Omega$ for $\gamma p \rightarrow \pi^0 N$ (GRAAL), 2 – the ΛK^+ recoil polarisation (CLAS), 3,4 – $d\sigma/d\Omega$ for $\gamma p \rightarrow \Sigma K$ reaction (SAPHIR, CLAS); b) the total χ^2 for all ΛK^+ and ΣK reactions.

tial cross sections. A rather shallow minimum is seen for the Λ recoil polarisation. The distribution of sum of χ^2 for all reactions with ΛK^+ and ΣK final states is shown in Fig. 16 b. The other state was found at (2166 ± 35) MeV, its width at (280 ± 65) MeV. With this resonance, the recoil polarisation in $\gamma p \rightarrow \Lambda K^+$ is described as well. Omitting this contribution from the fit yields the fit which is shown in Figs. 6 and 11 as dashed line. The mass scan of individual channels did not show a clear minimum for this state. The χ^2 for the recoil polarisation (differential cross section) show asymmetric minima, shallow on the high-mass (low-mass) side and steeper on the low-mass (high-mass) side. Only their sum gives a pronounced minimum in χ^2 .

3.4 The high mass range (> 2200 MeV)

At large photon energies, kaons are produced preferentially in forward direction. The forward peaks are well reproduced by the fit which assigns forward meson production to meson exchanges in the t -channel. In the mass range covered by CLAS and SAPHIR, the fractional contributions of the K and K^* exchanges are 8% and 22% to the total cross section for ΛK^+ and 25% and 47% for ΣK , respectively. In the $K^0 \Sigma^+$ differential cross section, there is no forward peak. The K reggeized exchange is supposed to be significantly suppressed, but the fit does not find a significant contribution from K^* exchange neither.

In the u -channel, Λ and Σ exchanges both contribute about 10% to ΛK^+ and to ΣK .

3.5 Discussion

3.5.1 Resonances with strong ΛK^+ , ΣK coupling

For $N(2000)F_{15}$ and $N(1870)D_{13}$ the masses were found to be about 70 MeV lower than in the previous analysis of data on $p\pi$ and $p\eta$ final states only [33,34]. As was pointed out in those publications, these resonances only weakly contributed to $p\pi$ and $p\eta$ cross sections and were helpful to describe the polarisation functions. In the present analysis we found that these states have significant couplings to ΣK and adding the $P_{11}(1840)$ state provided a flexibility to describe the polarisation data. The F_{15} state has now mass and width which are close to the values obtained by Höhler [45]. Moreover, the mass and width of his solution can be used as fixed input values without changing the quality of the description.

For ΛK^+ production, the S_{11} partial wave provides $(48 \pm 5)\%$ of the total cross section. The $N(1720)P_{13}$ contribution is the next strongest one with $(19 \pm 4)\%$. The newly observed states $N(1840)P_{11}$ and $N(2170)D_{13}$ contribute $3 \pm 1\%$ and $(2 \pm 0.8)\%$, respectively. For ΣK production, the S_{11} wave provides the strongest resonance contributions, $(22 \pm 6)\%$. The second strongest resonance is $D_{33}(1700)$ with $12 \pm 4\%$ while $N(1720)P_{13}$ contributes only about 1% to the cross section. The $N(1840)P_{11}$ and $N(2170)D_{13}$ resonances contribute on the level of 7% and 1% to the ΣK total cross section.

Although quite a large number of states contribute only weakly to the total cross sections, their amplitudes are important to describe the polarisation information. Here, the interference between large and small amplitudes can significantly change the polarisation function. The typical example is the beam asymmetry in the η photoproduction reaction where a small contribution from $N(1520)D_{13}$ changes the behaviour of the polarisation function dramatically.

3.5.2 Four D_{13} resonances

There are four nucleon resonances with quantum numbers $I(J^P) = 1/2(3/2)^-$ (D_{13}). These quantum numbers can be formed with intrinsic orbital angular momentum $L = 1$ and intrinsic spin $S = 1/2$, or with $S = 3/2$ and $L = 1$ or $L = 3$. The lowest mass state at 1520 MeV seems to be dominantly in a $(J = 3/2; L = 1, S = 1/2)$ state. Apart from $\Delta(1232)P_{33}$, it provides the largest contribution to the $p\pi^0$ photoproduction cross section. Its companion at 1700 MeV, dominantly $(J = 3/2; L = 1, S = 3/2)$, makes a much smaller contribution. It seems plausible that the two further states, $N(1870)D_{13}$ and $N(2170)D_{13}$, should have a dominantly $(J = 3/2; L = 1, S = 1/2)$ configuration. We note that the spacings in mass square are

$$M^2(2166) - M^2(1875) = (1.19 \pm 0.18) \text{ GeV}^2, \quad (3)$$

$$M^2(1875) - M^2(1520) = (1.20 \pm 0.10) \text{ GeV}^2, \quad (4)$$

which agrees with the N-Roper mass splitting

$$M^2(1440) - M^2(938) = (1.19 \pm 0.06) \text{ GeV}^2. \quad (5)$$

This leads to the conjecture that $N(1870)D_{13}$ and $N(2170)D_{13}$ could be the first and second radial excitation of the $N(1520)D_{13}$. It was shown in [46] that all sequential baryon resonances in a given partial wave have mass square spacings of about 1.142 GeV^2 .

3.5.3 Quark-model predictions for D_{13} resonances.

Quark-model calculations predict a very large number of states. This is exemplified here using the $N D_{13}$ resonance series and a comparison with the Bonn constituent-quark model [47]. The lowest mass states with negative parity have $L = 1$. The spatial wave function for $L = 1$ has mixed symmetry. Hence, the spin-flavour wave function has to have mixed symmetry, it has to belong to a 70-plet. A mixed symmetry spin-flavour wave function can be realised for $S = 1/2$ and $S = 3/2$. These two states can mix, thus forming the two states belonging to the $1 \hbar\omega$ band, $N(1520)D_{13}$ and $N(1700)D_{13}$.

In the third excitation band, the total orbital angular momentum can be $L = 1$ (with $S = 1/2, 3/2$) or $L = 3$ (with $S = 3/2$). Spatial wave functions can be constructed now which are symmetric, antisymmetric, or of mixed symmetry, resulting in a total of eight different states. They do not only mix among themselves; mixing

with higher configurations belonging to the fifth excitation band has to be considered as well. As a result, the Bonn model predicts $N D_{13}$ resonances at 1472 and 1622 MeV in the first excitation band and at 1918, 1988, 2146, 2170, 2190, 2223, 2231, and 2271 MeV in the third excitation band. (The quark model in [48] gives very similar results.) The underlined masses indicate those resonances which are dominantly spin 1/2 resonances within a 70-plet. It is conceivable that the photon couplings of these resonances are larger than those of other states. This conjecture could provide a natural explanation why $N(1870)D_{13}$ and $N(2170)D_{13}$ are observed and the other states not. However, model calculations of baryon decays do not reproduce this pattern. If the other resonances exist in addition, their discovery will require data of much higher statistics and additional polarisation data. New data from pion-induced reactions will likely be mandatory as well.

3.5.4 Do four S_{11} resonances exist?

There are claims for four nucleon resonances with quantum numbers S_{11} . A survey of these results can be found in [49]. The observation of the two high-mass states in photoproduction seems questionable since differential cross sections in the higher mass range are not well reproduced; in pion-induced reactions, the introduction of a third and fourth S_{11} resonance at (1846 ± 47) and (2113 ± 70) MeV improves data description considerably [50]. In this analysis, the two lowest mass states at 1535 and 1650 MeV are observed but we do not find any need for introducing additional S_{11} states. The pairs of resonances $N(1535)S_{11}$ and $N(1520)D_{13}$, $N(1846)S_{11}$ and $N(1870)D_{13}$, and $N(2133)S_{11}$ and $N(2170)D_{13}$, may provide reasonable spin doublets, with small spin-orbit splittings. Resonances belonging to spin triplets (or degenerate quartets) like $N(1650)S_{11}$ and $N(1700)D_{13}$ are only weakly excited and their radial excitations are not observed in the data discussed here.

4 Summary

Results of an analysis of hyperon photoproduction in the reactions $\gamma p \rightarrow \Lambda K^+$ and $\gamma p \rightarrow \Sigma K$ using data from the CLAS, LEPS and SAPHIR collaborations are presented. The data are analysed in a combined fit with data on π^0 and η photoproduction. The SAPHIR and the CLAS data are compatible only if a normalisation factor in the order of 0.85 is introduced. The combined fit yields results which are compatible with the results on π^0 and η photoproduction reported earlier by the CB-ELSA collaboration but requires to introduce new baryon resonances. In particular, a P_{11} state was observed in the region of 1840 MeV which contributes to almost all reactions. The analysis highlights the existence of four D_{13} resonances, $N(1520)D_{13}$, $N(1700)D_{13}$, $N(1870)D_{13}$, and $N(2170)D_{13}$. A comparison with the Bonn quark model suggests that the main component of their flavour wave functions all belong to 70-plets; the weakly excited $N(1700)D_{13}$ has dominantly intrinsic spin 3/2 while the other 3 resonances have mostly spin 1/2.

Acknowledgment

We would like to thank the CB-ELSA/TAPS collaboration for numerous discussions on topics related to this work. We acknowledge financial support from the Deutsche Forschungsgemeinschaft within the SFB/TR16. The St. Petersburg group received funds from the Russian Foundation for Basic Research (grant 04-02-17091). U. Thoma thanks for an Emmy Noether grant from the DFG. A. Anisovich and A. Sarantsev acknowledge support from the Alexander von Humboldt Foundation.

References

1. B. Krusche and S. Schadmand, Prog. Part. Nucl. Phys. **51** (2003) 399.
2. T. Meissner, F. Grummer, K. Goeke, and M. Harvey, Phys. Rev. D **39** (1989) 1903.
3. O. Krehl, C. Hanhart, S. Krewald, and J. Speth, Phys. Rev. C **62** (2000) 025207.
4. R. L. Jaffe and F. Wilczek, Phys. Rev. Lett. **91** (2003) 232003.
5. N. Kaiser, P. B. Siegel, and W. Weise, Phys. Lett. B **362** (1995) 23.
6. L. Y. Glozman and D. O. Riska, Phys. Lett. B **366** (1996) 305.
7. J. Caro Ramon, N. Kaiser, S. Wetzel and W. Weise, Nucl. Phys. A **672** (2000) 249.
8. S. Steininger and U. G. Meissner, Phys. Lett. B **391** (1997) 446.
9. D. Jido, J. A. Oller, E. Oset, A. Ramos, and U. G. Meissner, Nucl. Phys. A **725** (2003) 181.
10. N. Isgur, "Baryons: The promise, the problems, and the prospects", *7th International Conference on the Structure of Baryons*, (B.F. Gibson et al. eds.), Santa Fe, New Mexico, 3-7 Oct 1995 World Scientific, Singapore, 1996.
11. S. Capstick and W. Roberts, Phys. Rev. D **58** (1998) 074011.
12. K. H. Glander et al., Eur. Phys. J. A **19** (2004) 251.
13. J. W. C. McNabb et al., Phys. Rev. C **69** (2004) 042201.
14. R. G. T. Zegers et al., Phys. Rev. Lett. **91** (2003) 092001.
15. R. Lawall et al., Eur. Phys. J. A **24** (2005) 275.
16. T. Feuster and U. Mosel, Phys. Rev. C **58** (1998) 457.
17. T. Feuster and U. Mosel, Phys. Rev. C **59** (1999) 460.
18. G. Penner and U. Mosel, Phys. Rev. C **66** (2002) 055211.
19. G. Penner and U. Mosel, Phys. Rev. C **66**, (2002) 055212.
20. V. Shklyar, G. Penner, and U. Mosel, Eur. Phys. J. A **21** (2004) 445.
21. M. Guidal, J. M. Laget, and M. Vanderhaeghen, Phys. Rev. C **68** (2003) 058201.
22. T. Mart, C. Bennhold, H. Haberzettl and L. Tia-tor, "KaonMAID 2000" at www.kph.uni-mainz.de/MAID/kaon/kaonmaid.html.
23. T. Mart and C. Bennhold, Phys. Rev. C **61** (2000) 012201.
24. S. Janssen, J. Ryckebusch, W. Van Nespén, D. Debruyne, and T. Van Cauteren, Eur. Phys. J. A **11** (2001) 105.
S. Janssen, J. Ryckebusch, D. Debruyne, and T. Van Cauteren, Phys. Rev. C **65** (2002) 015201.
25. T. Mart, Phys. Rev. C **62** (2000) 038201.

26. T. Mart, A. Sulaksono and C. Bennhold, “Missing resonances in kaon photoproduction on the nucleon”, *International Symposium on Electrophoto Production of Strangeness on Nucleons and Nuclei (SENDAI 03)*, Sendai, Japan, 16-18 Jun 2003.
27. S. Janssen, J. Ryckebusch, D. Debruyne and T. Van Cauteren, *Phys. Rev. C* **66** (2002) 035202.
28. C. Bennhold, A. Waluyo, H. Haberzettl, T. Mart, G. Penner and U. Mosel, “Missing nucleon resonances in kaon production with pions and photons”, In: *Excited nucleons and hadronic structure*, Newport News 2000, 280 [arXiv:nucl-th/0008024].
29. B. Julia-Diaz, B. Saghai, F. Tabakin, W. T. Chiang, T. S. Lee and Z. Li, “Dynamical coupled-channel study of $K^+\Lambda$ photoproduction”, 10th International Conference on Structure of Baryons (Baryons 2004), Palaiseau, France, 25-29 Oct 2004. [arXiv:nucl-th/0501005].
30. D. Rebreyend *et al.*, *Nucl. Phys. A* **663** (2000) 436.
31. A. Usov and O. Scholten, “K Lambda and K Sigma photoproduction in a coupled channels framework”, submitted to *Phys. Rev. C*, [arXiv:nucl-th/0503013].
32. A. Anisovich, E. Klempt, A. Sarantsev, and U. Thoma, *Eur. Phys. J. A* **24** (2005) 111.
33. O. Bartholomy *et al.*, *Phys. Rev. Lett.* **94** (2005) 012003.
34. V. Crede *et al.*, *Phys. Rev. Lett.* **94** (2005) 012004.
35. B. Krusche *et al.*, *Phys. Rev. Lett.* **74** (1995) 3736.
36. GRAAL collaboration, article in preparation. We thank the GRAAL collaboration for providing their (preliminary) data to us prior to publication.
37. A. A. Belyaev *et al.*, *Nucl. Phys. B* **213** (1983) 201.
R. Beck *et al.*, *Phys. Rev. Lett.* **78** (1997) 606.
D. Rebreyend *et al.*, *Nucl. Phys. A* **663** (2000) 436.
38. J. Ajaka *et al.*, *Phys. Rev. Lett.* **81** (1998) 1797.
39. K. H. Althoff *et al.*, *Z. Phys. C* **18** (1983) 199.
E. J. Durwen, BONN-IR-80-7 (1980).
K. Buechler *et al.*, *Nucl. Phys. A* **570** (1994) 580.
40. A. V. Anisovich *et al.*, “Photoproduction of Baryons Decaying into $N\pi$ and $N\eta$ ”, preceding paper.
41. B. Carnahan, “Strangeness photoproduction in the $\gamma p \rightarrow K^0 \Sigma^+$ reaction”, UMI-31-09682 (microfiche), Ph.D. thesis (2003) at the Catholic University of America, Washington, D.C.
42. D. Diakonov and V. Petrov, *Phys. Rev. D* **69** (2004) 094011.
43. V. Kuznetsov *et al.*, “ η photoproduction off the neutron at GRAAL: Evidence for a resonant structure at $W = 1.67$ GeV”, Workshop on the Physics of Excited Nucleons (NSTAR 2004), Grenoble, France, 24-27 Mar 2004, [arXiv:hep-ex/0409032].
44. D. M. Manley and E. M. Saleski, *Phys. Rev. D* **45** (1992) 4002.
45. G. Höhler, “Determination of resonance pole parameters in πN scattering”, report, Karlsruhe (2004).
46. E. Klempt, *Phys. Rev. C* **66** (2002) 058201.
47. U. Löring, B. C. Metsch, and H. R. Petry, *Eur. Phys. J. A* **10** (2001) 395. We acknowledge several discussions with B. Metsch on this topic.
48. S. Capstick and W. Roberts, *Phys. Rev. D* **49** (1994) 4570.
49. B. Saghai, “Role of the baryon resonances in the η and K^+ photoproduction processes on the proton,” *Physics of Excited Nucleons*, NSTAR 2004 Workshop, Grenoble 2004, France, [arXiv:nucl-th/0408054].
50. G. Y. Chen, S. Kamalov, S. N. Yang, D. Drechsel, and L. Tiator, *Nucl. Phys. A* **723** (2003) 447.

Table 4. Changes in χ^2 when one of the new resonances is omitted or replaced by a resonance with different spin and parity J^P . The changes are given for the χ^2_{tot} (1) and the χ^2 contributions for individual final states calculated analogously.

Resonance	N(1840)P ₁₁				
	$\Delta\chi^2_{tot}$	$\Delta\chi^2_{p\pi^0}$	$\Delta\chi^2_{p\eta}$	$\Delta\chi^2_{\Lambda K^+}$	$\Delta\chi^2_{\Sigma K}$
J^P					
omitted	565	315	46	248	176
repl. by 1/2 ⁻	334	305	10	151	60
repl. by 5/2 ⁻	211	236	-6	64	158
repl. by 7/2 ⁻	462	269	32	222	167
repl. by 9/2 ⁻	291	208	17	158	32
repl. by 3/2 ⁺	434	301	28	257	4
repl. by 7/2 ⁺	516	305	45	177	155
repl. by 9/2 ⁺	468	191	54	216	73
Resonance	N(1870)D ₁₃				
	$\Delta\chi^2_{tot}$	$\Delta\chi^2_{p\pi^0}$	$\Delta\chi^2_{p\eta}$	$\Delta\chi^2_{\Lambda K^+}$	$\Delta\chi^2_{\Sigma K}$
J^P					
omitted	320	204	30	63	103
repl. by 1/2 ⁻	274	77	53	16	-21
repl. by 5/2 ⁻	129	97	11	-19	85
repl. by 7/2 ⁻	215	144	19	21	97
repl. by 9/2 ⁻	162	-29	37	28	63
repl. by 3/2 ⁺	262	43	57	-1	-13
repl. by 7/2 ⁺	164	154	11	8	23
repl. by 9/2 ⁺	204	87	35	-36	51
Resonance	N(2170)D ₁₃				
	$\Delta\chi^2_{tot}$	$\Delta\chi^2_{p\pi^0}$	$\Delta\chi^2_{p\eta}$	$\Delta\chi^2_{\Lambda K^+}$	$\Delta\chi^2_{\Sigma K}$
J^P					
omitted	311	161	6	368	59
repl. by 1/2 ⁻	206	59	1	385	-17
repl. by 5/2 ⁻	39	-77	-11	305	30
repl. by 7/2 ⁻	148	-28	-11	433	100
repl. by 9/2 ⁻	87	-52	0	292	-1
repl. by 1/2 ⁺	166	54	-6	330	48
repl. by 5/2 ⁺	149	136	-27	368	31
repl. by 7/2 ⁺	53	19	-5	127	17
repl. by 9/2 ⁺	133	94	-15	299	2

